

Influence of carbon nanocone structure on ultra-efficient water flow

Bruno H. S. Mendonça,^{*,†} Elizane E. de Moraes,^{‡,§} João P. K. Abal,[¶] João V. L. Valle,[‡] Tássylla O. Fonseca,[†] and Hélio Chacham[†]

[†]*Departamento de Física, ICEX, Universidade Federal de Minas Gerais, CP 702, Belo Horizonte 30123-970, MG, Brazil*

[‡]*Instituto de Física, Universidade Federal da Bahia, Campus Universitário de Ondina, Salvador 40210-340, BA, Brazil*

[¶]*Instituto de Física, Universidade Federal do Rio Grande do Sul, Porto Alegre 91501-970, RS, Brazil*

[§]*Catalan Institute of Nanoscience and Nanotechnology (ICN2), CSIC and BIST, Campus UAB, Bellaterra, 08193 Barcelona, Spain*

E-mail: brunnohenrique13@gmail.com

Abstract

In this study, using nonequilibrium molecular dynamics simulation, the water flow in carbon nanocones is studied using the TIP4P/2005 rigid water model. The results demonstrate a nonuniform dependence of the flow on the cone apex angle and the diameter of the opening where the flow is established, leading to a significant increase in the flow in some cases. The effects of cone diameter and pressure gradient are investigated to explain flow behavior with different system structures. We observed that some cones can optimize the water flow precisely. Nanocones with a larger opening facilitate the sliding of water, significantly increasing the flow, thus being promising membranes for technological use in water impurity separation

processes. Nanocones with narrower opening angles limited water mobility due to excessive confinement. This phenomenon is linked to the ability of water to form a larger hydrogen-bond network in typical systems with diameters of this size, obtaining a single-layer water structure. Nanocones act as selective nanofilters capable of allowing water molecules to pass through while blocking salts and impurities. The conical shape of their structures creates a directed flow that improves separation efficiency. Membranes based on carbon nanocones are becoming promising for clean, smart, and efficient technologies. The combination of transport speed, selectivity, and structural control put them ahead of other nanostructures for various purposes.

Introduction

The behavior of water at the nanoscale has recently attracted significant interest for engineering applications such as water desalination and purification. This interest stems from the enhanced interfacial effects of nanofluidic devices, where most fluid molecules interact with the surface.^{1–15} Consequently, constructing these devices from materials that facilitate rapid and efficient water transport is paramount. In the past decade, advances in the manipulation and manufacturing of nanomaterials have greatly improved, aiding in the identification of suitable materials and channel geometries and sizes that enhance water transport.^{7,8,16–22} Specifically, carbon allotropes, such as carbon nanotubes, graphite, and graphene, have emerged as potentially important materials in this field.^{23,24,24–30}

The phenomenon of enhanced water transport—often referred to as superflow—was notably reported by Qin et al.,¹⁶ who demonstrated that water confined in carbon nanotubes can flow up to 900 times faster than predicted by classical hydrodynamics. This discovery has spurred several research studies into low-friction nanomaterials such as graphene, graphitic surfaces, boron nitride nanotubes, and other nanomaterials.^{1,2,18,29–33,33–38} Among these, carbon nanocones (CNCs) have attracted increasing attention due to their sp^2 hybridization of graphene with a distinct conical morphology,^{39–46} which naturally resembles the hourglass-shaped structure of aquaporins (AQPs) - the biological channels responsible for highly efficient and selective water transport across cell mem-

branes.^{47,48} In AQPs, the narrow neck ensures selectivity, while the conical entrance reduces hydrodynamic resistance and improves permeability.^{47–50} Inspired by this natural design, CNCs offer a biomimetic pathway to achieve high water flux and selectivity in synthetic systems.³³ Recently, molecular dynamics studies by Leivas et al.^{51,52} demonstrated that hydrophilic carbon nanocones can efficiently capture water from both liquid and vapor phases, with enhanced performance under vapor exposure and scalability dependent on intercone spacing. In this context, the asymmetric shape of CNTS can also induce directional flow and reduce energy barriers, making them attractive candidates for nanofluidic devices and high-performance desalination membranes.

In this work, we performed a systematic study to investigate the effect of the structure of carbon nanocones on the water flow properties, using the classical approach of nonequilibrium molecular dynamics simulations. The water flow was related to the cones' opening angle, hydrogen bond breaking/forming capacity, flow, and the influence of the external pressure gradient to which the filtration system is subjected. The remainder of this manuscript is organized as follows: In Sec. II, we present the simulation methodology used in this analysis and define the simulated models. In Sec. III, we discuss the results, and in Sec. IV, we present the conclusions.

Simulation methodology

We used the non-equilibrium molecular dynamics method^{53,54} to simulate the transport of water from one reservoir through a carbon nanocone (CNC) membrane to another reservoir.^{55–59} The developed water reservoir system was based on the model proposed by Huang et al.⁶⁰ CNCs are conical structures that can theoretically be built by removing a sector from a circular graphene sheet, and reattaching the sheet in a conical shape. We considered, for the construction of the membranes, the five CNCs observed experimentally,⁴¹ with the following opening angles 19.2° , 38.9° , 60° , 84.6° and 112.9° , shown in Figure 1. The length of each nanocone L_C , as well as the number of pentagons N_P , the diameters R and r and the opening angle α , are detailed in Table 1.

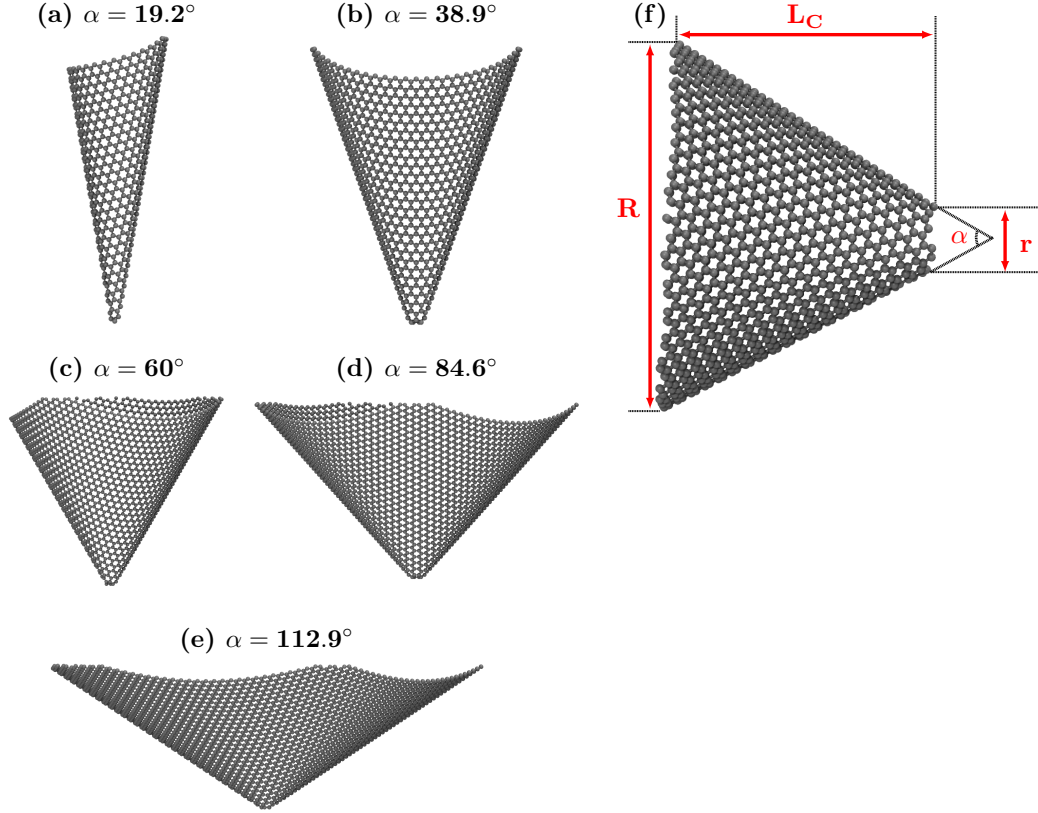


Figure 1: Snapshot of the carbon nanocones used in the simulations, with the following opening angles (a) 19.2° , (b) 38.9° , (c) 60° , (d) 84.6° , (e) 112.9° e (f) schematic showing of the parameters of the nanocone dimensions of interest.

Table 1: Parameters for the used carbon nanocones.

N_P	α	L_C (nm)	R (nm)	r (nm)
1	112.9°	4.37	8.08	0.86
2	84.6°	4.31	6.55	0.82
3	60°	4.28	5.09	0.81
4	38.9°	4.26	3.59	0.76
5	19.2°	4.43	2.17	0.76

Each carbon nanocone is connected, through its large and small openings, to nanopores in two parallel sheets of graphene with lateral lengths of $L_x = L_y = 10 \text{ nm}$. The diameter of the nanopore of each graphene sheet matches the diameter of one of the nanocone openings, so that the resulting systems consists of a conical hole in a bilayer graphene wall. The carbon nanocone axis was oriented parallel to the z axis, while the nanopore sheets were perpendicular to the z axis. Periodic

boundary conditions were used in all directions. In doing so, the simulation box must be large enough in the z direction to ensure that the molecules do not interact with each other across this boundary, so that the confined system is simulated correctly. We added two sheets of graphene with a length of $L_x = L_y = 10 \text{ nm}$ positioned at 10 nm on each side of the membrane opening that play the role of pistons, 1 and 2, applying pressure to the system. The pistons were oriented in the xy plane, perpendicular to the z axis. The z positions of the carbon atoms in the pistons were allowed to move along the z axis, while the relative position in the xy plane was fixed. The water molecules were confined in the space between the pistons and the membrane to create the two water reservoirs R_1 and R_2 . Each reservoir contains 5000 molecules of water. Piston 1 applies pressure in the water reservoir R_1 against the CNC membrane. The forces applied to the pistons are evenly distributed equal to the pressures specified for each reservoir, allowing the location z of the pistons to independently self-adjust to maintain the desired pressures and densities in each reservoir. During the simulation, it is important that the pistons remain well away from the inlet and outlet of the CNC membrane so as not to influence the flow through the channel. Pressures P_1 applied to piston 1 range from 200 to 1000 *bar* in intervals of 200 *bar*. The pressure P_2 applied to the piston 2 was 1 *bar*. This pressure difference creates a favorable environment for water molecules to be forced to pass from the higher pressure reservoir R_1 to the lower pressure reservoir R_2 . The difference in applied pressure generates a flow of water through the carbon nanocone. An external force applied to each carbon atom of the piston generated motion in the z direction. The pressure exerted by the piston on the water was calculated using the equation $P = \frac{Fn}{A}$, where P is the desired pressure applied by the piston, F is the force applied to each atom in the direction z , n is the number of carbon atoms in each piston, and A is the surface area of the piston. The described system is shown in Figure 2.

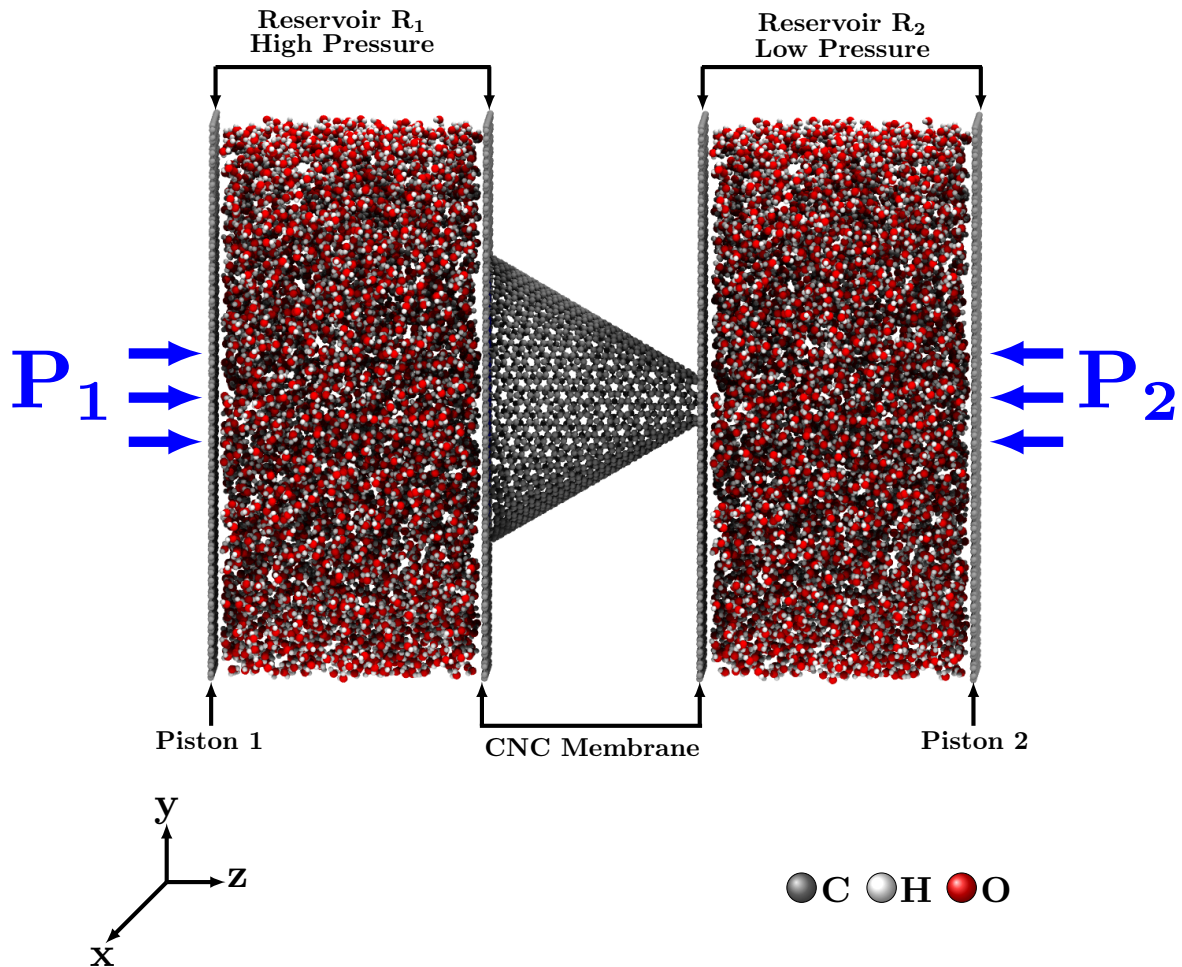


Figure 2: The constructed system used in this work. A snapshot of the dual reservoir system shows the graphene pistons and the carbon nanocone membrane in the center. Graphene pistons 1 and 2 apply pressure P_1 and P_2 to the fluid. The blue arrows indicate the direction in which the pistons apply force to the water reservoirs, R_1 and R_2 . The water flow was created by applying a pressure to reservoir R_1 that is greater than the pressure applied to reservoir R_2 . The water molecules appear as a red oxygen atom connected to two white hydrogen atoms, and the carbon molecules in shades of gray.

The SHAKE⁶¹ algorithm is employed to stabilize the molecule bonds and angles. The nanocones and the graphene sheets are modeled by the Lennard-Jones potential (LJ) considering fixed bond lengths and angles⁶² with effective carbon-carbon interaction energy $\epsilon_{CC} = 0.086 \text{ kcal}\cdot\text{mol}^{-1}$ and an effective diameter of $\sigma_{CC} = 3.4 \text{ \AA}$.⁶³ The carbon-oxygen energy $\epsilon_{CO} = 0.11831 \text{ kcal}\cdot\text{mol}^{-1}$ and the effective carbon-oxygen diameter $\sigma_{CO} = 3.28218 \text{ \AA}$.⁶³ The Lorentz-Berteloth mixing rules provided the LJ crossing parameters.

The parameters considered for the water model were defined and are shown in Table 2. In this water model, the Lennard-Jones site is located on the oxygen atom, with parameters σ and ϵ . The charges of oxygen and hydrogen are q_O and q_H , respectively. The TIP4P/2005 model places a negative charge q_M at a point M at a distance d_{OM} from the oxygen along the H-O-H bisector. The distance between the oxygen and hydrogen sites is r_{OH} . The angle formed between hydrogen, oxygen, and another hydrogen atom is given by θ_{HOH} .

Table 2: Parameters of the TIP4P/2005 force field used for the water models.

ϵ_{OO} (kcal mol ⁻¹)	0.1852
ϵ_{HH} (kcal mol ⁻¹)	0.0
σ_{OO} (Å)	3.1589
σ_{HH} (Å)	0.0
q_O (e)	0.0
q_H (e)	0.5564
q_M (e)	-1.1128
d_{OM} (Å)	0.1546
r_{OH} (Å)	0.9572
θ_{HOH} (°)	104.52

The simulations were performed with the Large-scale Atomic/Molecular Massively Parallel Simulator (LAMMPS)⁶⁴ package. We employ the Particle-Particle Particle-Mesh (PPPM) method to calculate long-range Coulomb interactions.⁶⁵ This method deals with the long-range interactions and the Coulomb field of real charges in a way that can interfere with its own images. We got around this problem by creating a simulation box on the z axis around 500 nm for all systems, avoiding interaction with their own images and making it impossible to superimpose virtual images with real images, minimizing possible errors in the application of the method.

The simulation protocol involves the following steps:

1. Pre-equilibrium in the NVE ensemble with a 0.5 ns MD run to minimize system energy keeping the pistons frozen (net force equal to zero).
2. Forces are applied in the pistons in order to impose 1 bar in each system to reach the water equilibrium densities at 300 K. Equilibration in the NPT ensemble during 1.0 ns.

3. The pistons are frozen in the new equilibrium position. Equilibration in the NVT ensemble at 300 K controlled via the Nosé-Hoover thermostat⁶⁶ during 2.0 ns.
4. Nanopores are opened. Different forces are applied in each piston to mimic the pressure gradient. NPT ensemble during 10 ns at 300 K and different feed pressures.

The system's dynamics features were evaluated by considering the flow rate calculations as given by the equation $\phi_{H_2O} = Av$, where A is the graphene layer area ($3.4 \times 3.4 \text{ nm}^2$), and v is the velocity of water flow acquired from the least-square linear regression line fitted to the data cloud which relates the mean molecular displacement along the tube axis as a function of time taken from the MD trajectory file.

Results and discussion

Molecular dynamics simulations show that water flows through carbon nanocones significantly faster than through nanotubes of the same length and similar diameters, as we show in Fig. 3. We observed that the flow of water confined in carbon nanotubes is more uniform than in nanocones, and the water tends to organize itself into rows or chains, especially for nanotubes of small diameter. In nanocones, we observed flow magnitudes that are one order of magnitude larger than in nanotubes with similar structural properties.² The nanocone flow enhancement is driven by the conical shape itself, which creates a pressure gradient that naturally drives the water flow. The conical shape of the nanocones favors spontaneous pressure gradients and nearly frictionless sliding, promoting superflow of water - at a speed much higher than expected by classical hydrodynamic models.

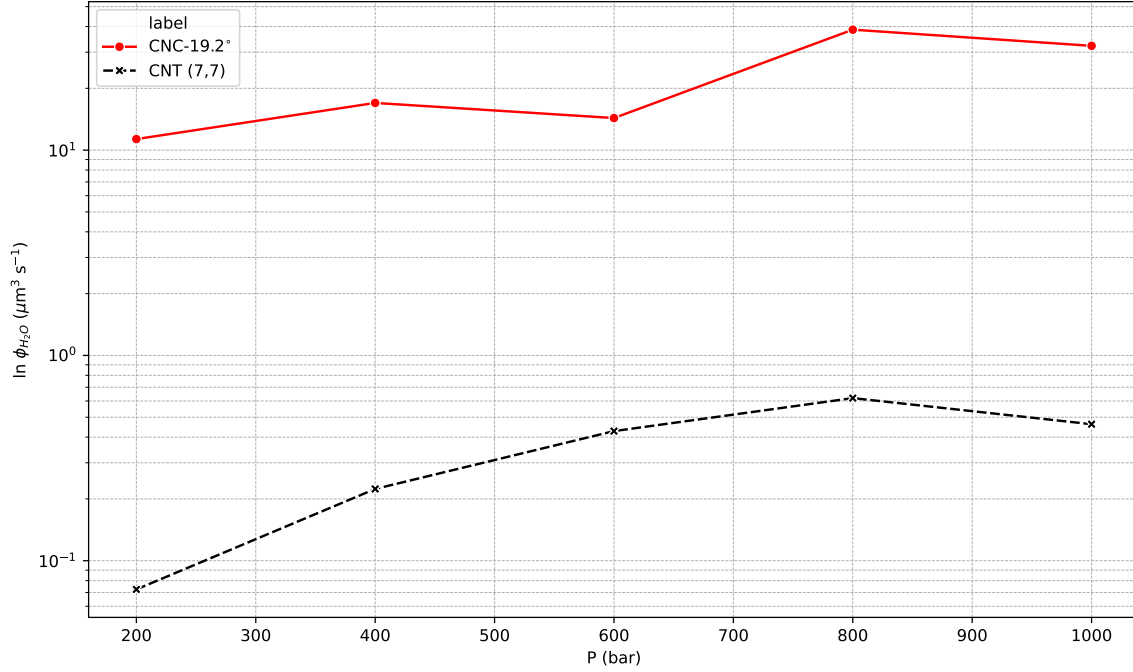


Figure 3: Log of the flow rate as a function of the pressure gradient applied to the carbon nanocone CNC-19.2° and carbon nanotube (7, 7).

We analyzed all experimentally characterized carbon nanocone structures.^{41,67} Depending on the number of pentagons at the apex of the CNC,⁶⁸ there are five symmetric CNCs with apex angles of CNC-112.9°, CNC-84.6°, CNC-60°, CNC-38.9°, and CNC-19.2°. Here, the tips of the CNCs were cut (Fig. 1) and their accessible pore areas are shown in Fig. 1 and described in Table 1.

First, we studied the water flow under different hydrostatic pressures in all CNCs. An approximately linear relationship between pressure and water flow was observed for all systems. Therefore, to obtain sufficient statistics in a limited simulation time, hydrostatic pressures from 200 bar to 1000 bar were adopted in the following simulations. Using these conditions, we examined the water flow performance of the systems shown in Fig. 2.

The calculated flow rates are shown in Fig. 4 as a function of pressure gradient, for several cone structures. The flow rate increases enormously with cone apex angle, resulting in increases of more than one order of magnitude for a given pressure gradient. When water flows in CNCs from

the larger opening to the smaller opening, the mobility of water molecules increases smoothly, allowing more water to enter, which contributes to their higher water flux as the CNC opening increases. Similarly, when water flows in the opposite direction, it can easily diffuse out, which also provides relatively lower flows. The larger pores on the base side in CNCs and the corresponding higher probability of collecting water from the solution under pressure are possibly responsible for the higher water fluxes going from the larger diameter to the smaller one, which explains the obtained results.

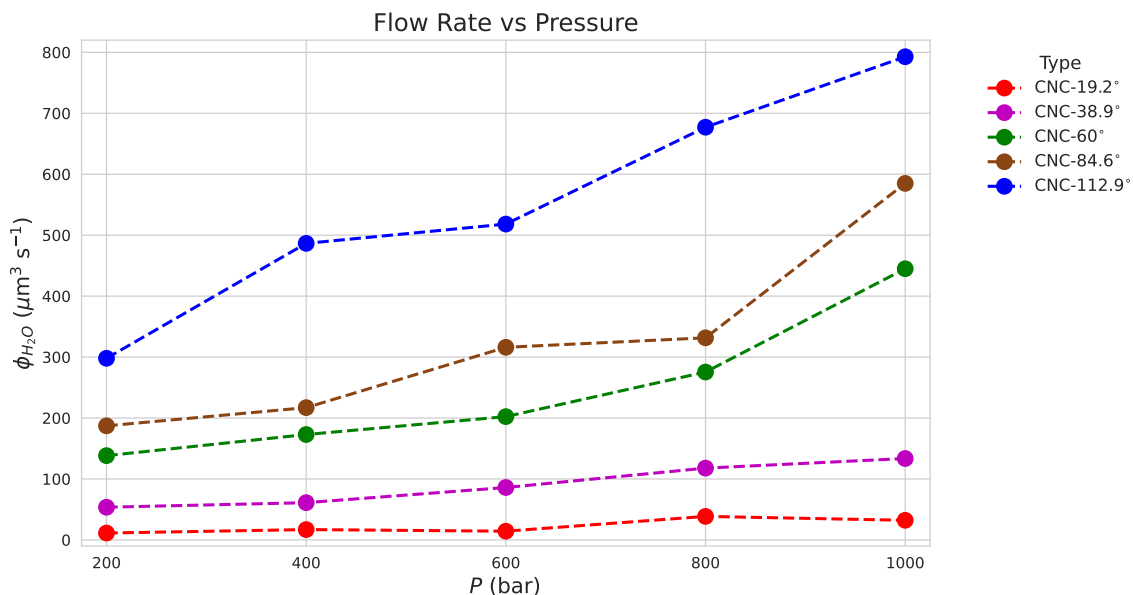


Figure 4: Flow rate as a function of the pressure gradient applied to the carbon nanocones.

Figs. 5 and 6 show the water density maps of the simulated systems. In the CNC-19.2° system, the water is relatively ordered (Fig. 5 (a-e) and Fig. 6 (a-e)), and consequently the water fluxes in this CNC are small. When the apex angle is increased, the water molecules become less ordered, as in bulk water, causing an increase in their flux. We can observe this from CNC-38.9° onwards.¹

It should be noted that in our simulations, all carbon atoms in CNC channels are electroneutral. However, in a real system, carbon atoms at the edge of CNC channels are prone to be oxidized and develop small net charges. The net charges can polarize the passing water molecules and cause the water molecules to reorient. Therefore, we believe that the small net charges and the corresponding

ordered water structure can further enhance the water flux^{69,70}

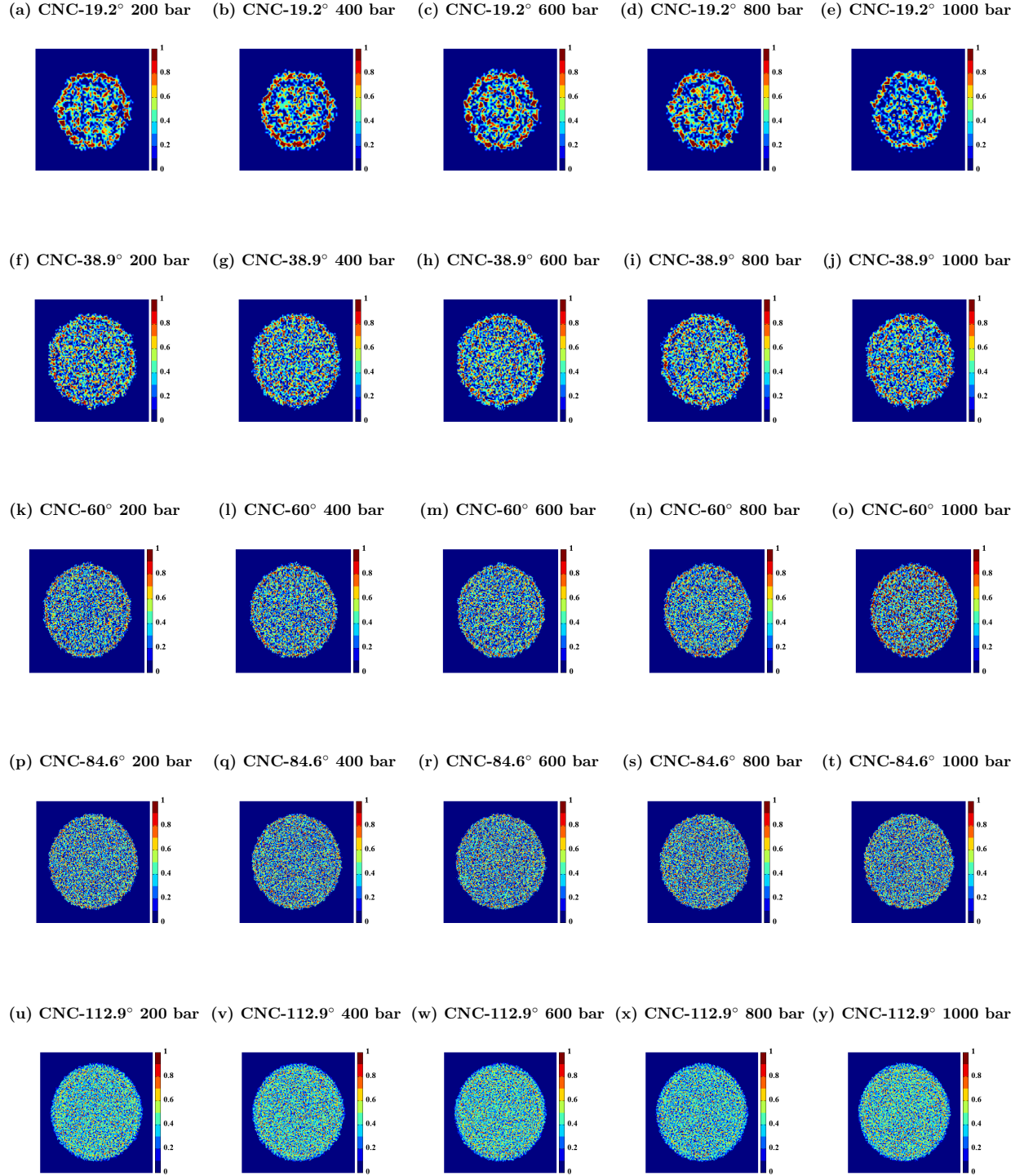
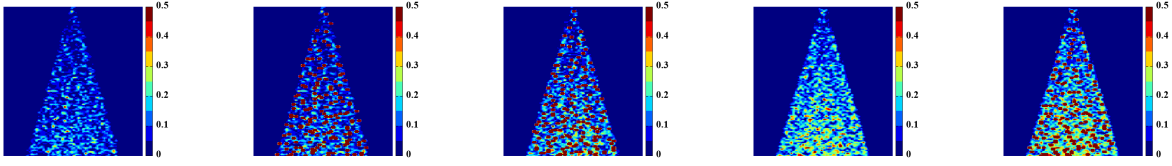
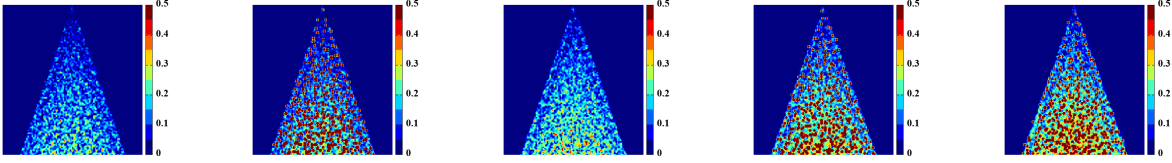


Figure 5: Density maps in the xy direction for the carbon nanocones. Dark blue regions have a low probability of finding water molecules, while red regions have a high probability of finding water molecules.

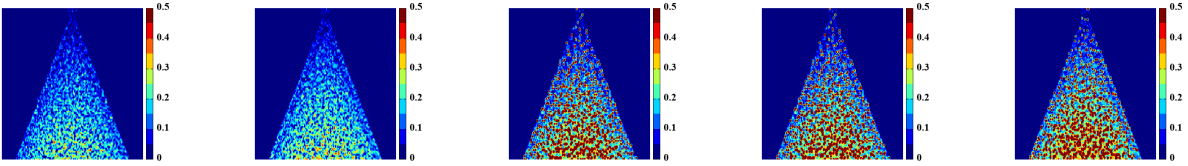
(a) CNC-19.2° 200 bar (b) CNC-19.2° 400 bar (c) CNC-19.2° 600 bar (d) CNC-19.2° 800 bar (e) CNC-19.2° 1000 bar



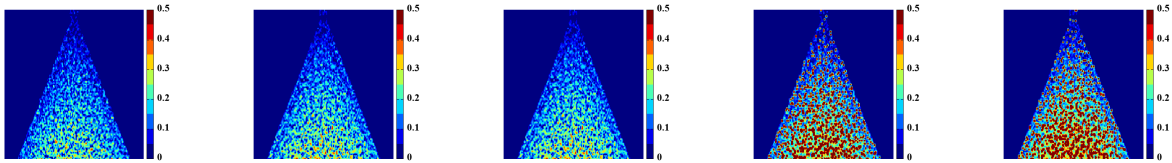
(f) CNC-38.9° 200 bar (g) CNC-38.9° 400 bar (h) CNC-38.9° 600 bar (i) CNC-38.9° 800 bar (j) CNC-38.9° 1000 bar



(k) CNC-60° 200 bar (l) CNC-60° 400 bar (m) CNC-60° 600 bar (n) CNC-60° 800 bar (o) CNC-60° 1000 bar



(p) CNC-84.6° 200 bar (q) CNC-84.6° 400 bar (r) CNC-84.6° 600 bar (s) CNC-84.6° 800 bar (t) CNC-84.6° 1000 bar



(u) CNC-112.9° 200 bar (v) CNC-112.9° 400 bar (w) CNC-112.9° 600 bar (x) CNC-112.9° 800 bar (y) CNC-112.9° 1000 bar

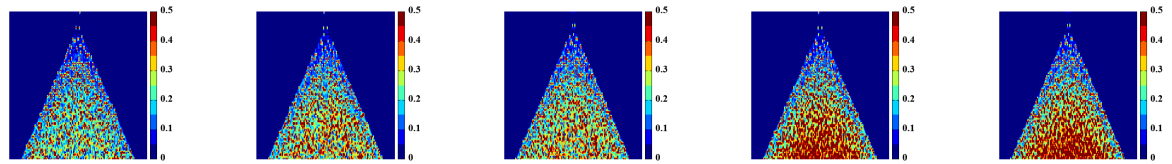


Figure 6: Density maps in the yz direction for the carbon nanocones. Dark blue regions have a low probability of finding water molecules, while red regions have a high probability of finding water molecules.

We also investigated the dependence of water transport on one main aspect: the hydrogen bonding behavior of confined water molecules. Fig. 7 shows that the absolute number of hydrogen bonds per molecule within the nanocone does not vary substantially across different structures. However, a more detailed assessment revealed that each nanocone geometry exhibits a distinct number of broken hydrogen bonds relative to the entry region.

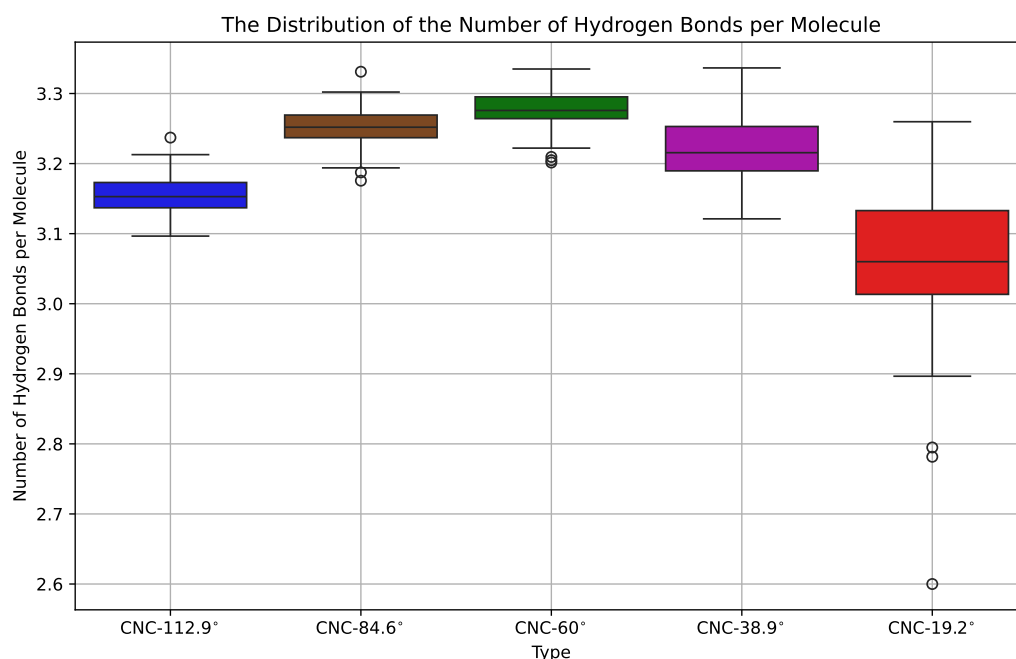


Figure 7: The distribution of the number of hydrogen bonds per molecule as boxplot and by each carbon nanocones structure.

The percentage of hydrogen bonds broken were obtained by dividing each nanocone into three equally high sections—namely, the entry (first slice), the middle (middle slice), and the exit (final slice) regions. As shown in Fig. 8, when comparing the number of hydrogen bonds in the middle and final slices to those in the entry region, structure CNC-19.2° presents a substantially larger drop in hydrogen bonds. This steep decline indicates that water molecules traversing CNC-19.2° must, on average, break a greater number of hydrogen bonds to move from one region to the next. Such enhanced bond disruption likely translates into a higher energy barrier for molecular

transport, thereby contributing to the lower flux in the CNC-19.2° configuration.

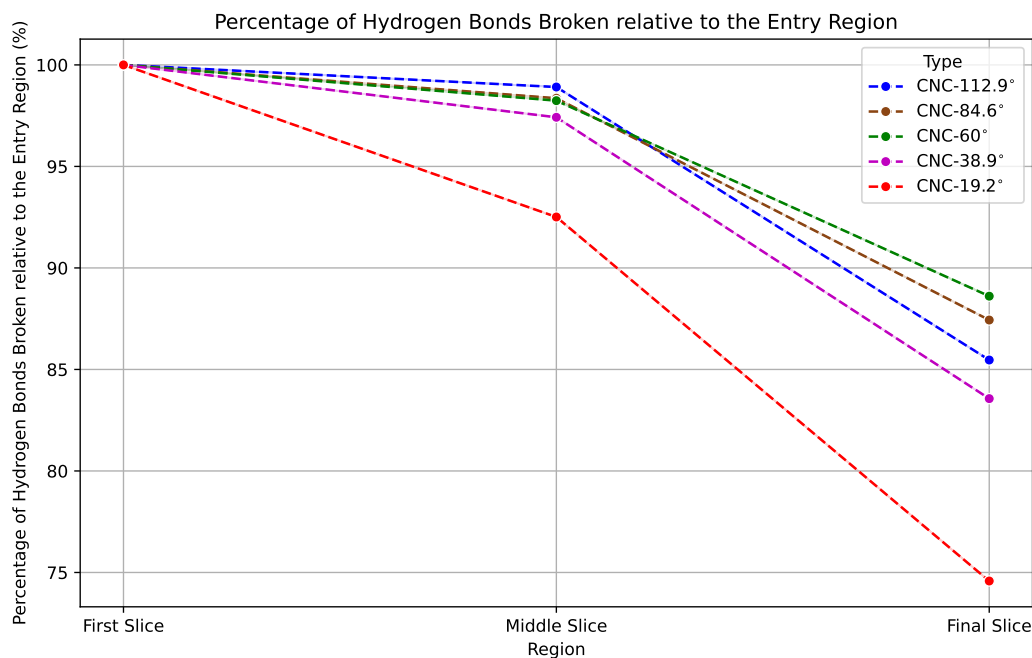


Figure 8: The percentage of hydrogen bonds broken relative to the carbon nanocones entry region for each carbon nanocones structure.

In summary, our simulations reveal that while the overall hydrogen bonding network of confined water does not dramatically differ among the CNC structures, the interplay within the local hydrogen bond dynamics is crucial. The higher number of hydrogen bonds broken along the structure CNC-19.2° result in a more rigid and structured water network that, in turn, impedes flux. Conversely, structures with lower percentage of hydrogen bonds broken presents more gradual change in hydrogen bonding along the cone and that allow water molecules to traverse the nanocone with less disruption. These insights provide a intereseting understanding of how nanoscale geometric parameters can be manipulated to optimize fluid transport in confined systems, which is pivotal for the design of efficient nanofluidic devices.

Conclusions

In this work, molecular dynamics simulations were conducted to investigate the performance of confined water flow in CNC membranes. The results show that CNCs can closely optimize water flow depending on the diameter of the CNC. In addition, CNC with an apex angle of 19.2° provides the lowest water flow, due to a greater ordering of the water present in the channel, a fact that is linked to the ability of water to form a larger hydrogen bond network in typical systems with diameters of this size, obtaining a single-layer water structure. Under pressure, CNCs also exhibit better water flow performance as we increase the apex angle of the CNCs, for these systems we have a typical water mobility behavior of bulk water. An application of these systems would be the fabrication of membranes to be used in water desalination processes. Water flow in CNCs has enormous technological potential because of its unique properties of superflux, extreme confinement, and low friction. Therefore, the fabrication of CNC membranes with uniform configuration and precise pore sizes for desalination will become a reality in the near future. Carbon nanocones are becoming a promising platform for clean, smart, and efficient technologies. The combination of transport speed, selectivity, and structural control put them ahead of other nanostructures for various purposes. This work offers great promise for the next generation of desalination devices.

Acknowledgement

This work is funded by the Brazilian scientific agency Conselho Nacional de Desenvolvimento Científico e Tecnológico (CNPq), Fundação de Amparo à Pesquisa do Estado da Bahia (FAPESB), and the Brazilian Institute of Science and Technology (INCT) in Carbon Nanomaterials with collaboration and computational support from Universidade Federal de Minas Gerais (UFMG) and Universidade Federal da Bahia (UFBA). BHSM thanks Rede Mineira de Materiais Bidimensionais (REDE 2D) and the science agency Fundação de Amparo à Pesquisa do Estado de Minas Gerais (FAPEMIG) for financial support. EEM appreciates Edital PRPPG 010/2024 Programa de Apoio a Jovens Professores(as)/Pesquisadores(as) Doutores(as) - JOVEMPESQ Project 24460. Finally,

authors acknowledge the National Laboratory for Scientific Computing (LNCC/MCTI, Brazil) for providing HPC resources of the SDumont supercomputer, which have contributed to the research results reported within this paper. URL: <http://sdumont.lncc.br>.

References

- (1) Li, W.; Wang, W.; Zhang, Y.; Yan, Y.; Král, P.; Zhang, J. Highly efficient water desalination in carbon nanocones. *Carbon* **2018**, *129*, 374–379.
- (2) Mendonça, B. H.; de Moraes, E. E.; Kirch, A.; Batista, R. J.; de Oliveira, A. B.; Barbosa, M. C.; Chacham, H. Flow through deformed carbon nanotubes predicted by rigid and flexible water models. *The Journal of Physical Chemistry B* **2023**, *127*, 8634–8643.
- (3) Losey, J.; Kannam, S. K.; Todd, B.; Sadus, R. J. Flow of water through carbon nanotubes predicted by different atomistic water models. *The Journal of Chemical Physics* **2019**, *150*, 194501.
- (4) Mendonça, B. H.; de Moraes, E. E.; Batista, R. J.; de Oliveira, A. B.; Barbosa, M. C.; Chacham, H. Water diffusion in carbon nanotubes for rigid and flexible models. *The Journal of Physical Chemistry C* **2023**,
- (5) Valle, J. V.; Mendonça, B. H.; Barbosa, M. C.; Chacham, H.; de Moraes, E. E. Accuracy of tip4p/2005 and spc/fw water models. *The Journal of Physical Chemistry B* **2024**, *128*, 1091–1097.
- (6) Rashidi, R.; Wu, T.; Sun, C.; Peeters, F.; Neek-Amal, M. Slip length and rapid fluid flow in hybrid nanochannels. *Physics of Fluids* **2024**, *36*.
- (7) Yasmeen, R.; Khan, F. S.; Nisa, W. U.; Saleem, A. R.; Awais, M.; Jameel, M.; Dara, R. N., et al. Enhanced water purification by using graphene oxide nano-membranes: A novel approach for mitigating industrial pollutant. *Carbon Trends* **2025**, *19*, 100486.

- (8) Karim, K. E.; Barisik, M.; Bakli, C.; Kim, B. Estimating water transport in carbon nanotubes: A critical review and inclusion of scale effects. *Physical Chemistry Chemical Physics* **2024**,
- (9) Zhang, S.; Song, R.; Zeng, H.; Wu, N.; Duan, H.; Wang, L. Exploring anomalous nanofluidic transport at the interfaces. *Droplet* **2024**, 3, e110.
- (10) Tan, R.; Shao, H.; Wan, Z.; Li, Y.; Gu, J.; Jia, R.; Hong, Z.; Ji, Z.; Zhang, S.; Li, X., et al. De novo contrived three-in-one oriented graft molecule for high-performance GO nanofiltration membranes with ultra-low friction 2D nanochannels. *Journal of Membrane Science* **2024**, 709, 123151.
- (11) Mendonça, B. H.; de Freitas, D. N.; Köhler, M. H.; Batista, R. J.; Barbosa, M. C.; de Oliveira, A. B. Diffusion behaviour of water confined in deformed carbon nanotubes. *Physica A: Statistical Mechanics and its Applications* **2019**, 517, 491–498.
- (12) de Freitas, D. N.; Mendonça, B. H.; Köhler, M. H.; Barbosa, M. C.; Matos, M. J.; Batista, R. J.; de Oliveira, A. B. Water diffusion in carbon nanotubes under directional electric fields: Coupling between mobility and hydrogen bonding. *Chemical Physics* **2020**, 537, 110849.
- (13) Mendonça, B. H.; Ternes, P.; Salcedo, E.; de Oliveira, A. B.; Barbosa, M. C. Water diffusion in carbon nanotubes: Interplay between confinement, surface deformation, and temperature. *The Journal of Chemical Physics* **2020**, 153.
- (14) Mendonça, B. H.; Ternes, P.; Salcedo, E.; de Oliveira, A. B.; Barbosa, M. C. Water diffusion in rough carbon nanotubes. *The Journal of Chemical Physics* **2020**, 152.
- (15) Mendonça, B. H.; Pereira, N.; Rezende, N. P.; Moraes, E. E. d.; Lacerda, R. G.; Chacham, H. Conduction Percolation in MoS₂ Nanoink Humidity Sensors: Critical Exponents and Nanochannel Dimensionality. *The Journal of Physical Chemistry C* **2024**, 128, 8042–8047.

- (16) Qin, X.; Yuan, Q.; Zhao, Y.; Xie, S.; Liu, Z. Measurement of the rate of water translocation through carbon nanotubes. *Nano Letters* **2011**, *11*, 2173–2177.
- (17) Ebrahim, A.; Kandasamy, S.; Isleem, H. F.; Khan, A. H.; Prasad, C.; Mohammed, A. S.; Alyaseen, A. Synergistic effects of combined multi-walled carbon nanotubes and glass fibers on concrete: experimental and economic analysis. *Fullerenes, Nanotubes and Carbon Nanostructures* **2024**, 1–17.
- (18) Abal, J. P.; Dillenburg, R. F.; Kohler, M. H.; Barbosa, M. C. Molecular dynamics simulations of water anchored in multilayered nanoporous MoS₂ membranes: implications for desalination. *ACS Applied Nano Materials* **2021**, *4*, 10467–10476.
- (19) Kim, C.-M.; Yang, E.; Karnik, R.; Field, R. W.; Fane, A. G.; Wang, P.; Kim, I. S. Transition of water transport mechanism in laminar graphene membrane with increasing thickness: Influence of strong cohesive interaction among water molecules. *Chemical Engineering Journal* **2025**, *505*, 158366.
- (20) Lockerby, D. A. First-order analysis of slip flow for micro and nanoscale applications. *Flow* **2025**, *5*, E3.
- (21) Xia, Q.; Pan, Y.; Liu, B.; Zhang, X.; Li, E.; Shen, T.; Li, S.; Xu, N.; Ding, J.; Wang, C., et al. Solar-driven abnormal evaporation of nanoconfined water. *Science Advances* **2024**, *10*, eadj3760.
- (22) Yang, Y.; Gao, Q.; Liang, W.; Zhang, X.; Qian, L.; Li, Z.; Chen, X. Enhanced Stretchable 2D Metal-Graphene Membranes with Superior Mechanical Properties for Sieving Lithium from Brine. *Small* **2024**, 2409950.
- (23) Qiao, R.; Aluru, N. R. Ion concentrations and velocity profiles in nanochannel electroosmotic flows. *The Journal of Chemical Physics* **2003**, *118*, 4692–4701.

- (24) Saedi, L.; Jameh-Bozorghi, S.; Maskanati, M.; Soleymanabadi, H. The effect of water on the electronic and field emission properties of inorganic AlN nanocones: computational study. *Inorganic Chemistry Communications* **2018**, *90*, 86–91.
- (25) Singh, E.; Osmani, R. A. M.; Banerjee, R. *Membrane-Based Hybrid Processes for Wastewater Treatment*; 2021; pp 657–691.
- (26) Ebrahimi, F.; Ramazani, F.; Sahimi, M. Nanofunction effects on water flow in carbon nanotubes. *Scientific Reports* **2018**, *8*, 7752.
- (27) Singh, S.; Gupta, K.; Sharma, M.; Kaur, H.; Sharma, N. K. Desalination of Wastewater Using Bio-nanomaterials. *Bio-Nanomaterials in Environmental Remediation: Industrial Applications* **2025**, 105–132.
- (28) Sahu, P.; Ali, S. M.; Kumar, V.; Duggal, V. Large scale molecular dynamics simulations for sea water desalination using nanotube membrane. *Journal of Molecular Liquids* **2025**, *418*, 126705.
- (29) Li, H.; Wang, S.; Zheng, J.; Wang, J. Electric Field Modulation of Water Transport in Carbon Nanotubes: Insights from Molecular Dynamics Simulations. *The Journal of Physical Chemistry C* **2024**, *128*, 21190–21200.
- (30) Li, Y.; Li, Z.; Misra, R. P.; Liang, C.; Gillen, A. J.; Zhao, S.; Abdullah, J.; Laurence, T.; Fagan, J. A.; Aluru, N., et al. Molecular transport enhancement in pure metallic carbon nanotube porins. *Nature Materials* **2024**, *23*, 1123–1130.
- (31) Suk, M. E.; Aluru, N. R. Water transport through ultrathin graphene. *The Journal of Physical Chemistry Letters* **2010**, *1*, 1590–1594.
- (32) Li, Z.; Han, Q.; Qiu, Y.; Wang, D. Modulation of water transport in carbon nanotubes by local charges. *Carbon* **2023**, *202*, 83–92.

- (33) Sun, Z.; Wang, S.; Xiong, H.; Wu, K.; Shi, J. Optimal nanocone geometry for water flow. *AIChE Journal* **2022**, *68*, e17543.
- (34) Thomas, J. A.; McGaughey, A. J. Water flow in carbon nanotubes: transition to subcontinuum transport. *Physical Review Letters* **2009**, *102*, 184502.
- (35) Kargar, M.; Lohrasebi, A. Water flow modeling through a graphene-based nanochannel: Theory and simulation. *Physical Chemistry Chemical Physics* **2019**, *21*, 3304–3309.
- (36) Zhou, R.; Neek-Amal, M.; Peeters, F. M.; Bai, B.; Sun, C. Interlink between abnormal water imbibition in hydrophilic and rapid flow in hydrophobic nanochannels. *Physical Review Letters* **2024**, *132*, 184001.
- (37) Yang, D.-C.; Castellano, R. J.; Silvy, R. P.; Lageshetty, S. K.; Praino, R. F.; Fornasiero, F.; Shan, J. W. Fast water transport through subnanometer diameter vertically aligned carbon nanotube membranes. *Nano Letters* **2023**, *23*, 4956–4964.
- (38) Paul, A.; Aluru, N. Surge-protected mechanical amplifier of ion transport devised using a bipolar nanopore with broken symmetry. *Physical Review E* **2025**, *111*, L023101.
- (39) Naess, S. N.; Elgsaeter, A.; Helgesen, G.; Knudsen, K. D. Carbon nanocones: wall structure and morphology. *Science and Technology of Advanced Materials* **2009**, *10*, 065002.
- (40) Charlier, J.-C.; Rignanese, G.-M. Electronic structure of carbon nanocones. *Physical Review Letters* **2001**, *86*, 5970.
- (41) Krishnan, A.; Dujardin, E.; Treacy, M.; Hugdahl, J.; Lynum, S.; Ebbesen, T. Graphitic cones and the nucleation of curved carbon surfaces. *Nature* **1997**, *388*, 451–454.
- (42) Jordan, Y. A. B.; Sead, F. F.; Sur, D.; Ballal, S.; Singh, A.; Krithiga, T.; Kubaev, A.; Ray, S.; Bekhit, M. M. DFT study of pure and Pt-decorated BN nanocone as a nanocarrier for nitrosourea anticancer drug. *Journal of Molecular Graphics and Modelling* **2025**, *137*, 109018.

- (43) Mistry, S.; Pillai, R.; Mattia, D.; Borg, M. K. Untangling the physics of water transport in boron nitride nanotubes. *Nanoscale* **2021**, *13*, 18096–18102.
- (44) Chen, K.-T.; Li, Q.-Y.; Takahashi, K. Slip flow on graphene: current status and perspective. *Journal of Thermal Science* **2022**, *31*, 1115–1134.
- (45) Feng, J.; Graf, M.; Liu, K.; Ovchinnikov, D.; Dumcenco, D.; Heiranian, M.; Nandigana, V.; Aluru, N. R.; Kis, A.; Radenovic, A. Single-layer MoS₂ nanopores as nanopower generators. *Nature* **2016**, *536*, 197–200.
- (46) Gol, A. G.; Akbari, J.; Khalaj, M.; Mousavi-Safavi, S. M.; Esfahani, S.; Farahani, N. DFT investigation of a Zn-doped carbon nanocone for the drug delivery of methylated aspirins. *Computational and Theoretical Chemistry* **2023**, *1220*, 113976.
- (47) Agre, P. Aquaporin water channels (Nobel lecture). *Angewandte Chemie International Edition* **2004**, *43*, 4278–4290.
- (48) Barati Farimani, A.; Aluru, N.; Tajkhorshid, E. Thermodynamic insight into spontaneous hydration and rapid water permeation in aquaporins. *Applied Physics Letters* **2014**, *105*.
- (49) Ho, J. D.; Yeh, R.; Sandstrom, A.; Chorny, I.; Harries, W. E.; Robbins, R. A.; Miercke, L. J.; Stroud, R. M. Crystal structure of human aquaporin 4 at 1.8 Å and its mechanism of conduction. *Proceedings of the National Academy of Sciences* **2009**, *106*, 7437–7442.
- (50) Gravelle, S.; Joly, L.; Ybert, C.; Bocquet, L. Large permeabilities of hourglass nanopores: From hydrodynamics to single file transport. *The Journal of Chemical Physics* **2014**, *141*.
- (51) Leivas, F. R.; Barbosa, M. C. Atmospheric water harvesting using functionalized carbon nanocones. *Beilstein Journal of Nanotechnology* **2023**, *14*, 1–10.
- (52) R Leivas, F.; Barbosa, M. C. Functionalized carbon nanocones performance in water harvesting. *The Journal of Chemical Physics* **2023**, *158*.

- (53) Alder, B. J.; Wainwright, T. E. Phase transition for a hard sphere system. *The Journal of Chemical Physics* **1957**, *27*, 1208–1209.
- (54) Alder, B. J.; Wainwright, T. E. Studies in molecular dynamics. I. General method. *The Journal of Chemical Physics* **1959**, *31*, 459–466.
- (55) Losey, J.; Kannam, S. K.; Todd, B.; Sadus, R. J. Flow of water through carbon nanotubes predicted by different atomistic water models. *The Journal of Chemical Physics* **2019**, *150*, 194501.
- (56) Kleinubing Abal, J. P.; Barbosa, M. C. Molecular fluid flow in MoS₂ nanoporous membranes and hydrodynamics interactions. *The Journal of Chemical Physics* **2021**, *154*, 134506.
- (57) Abal, J. P.; Dillenburg, R. F.; Kohler, M. H.; Barbosa, M. C. Molecular Dynamics Simulations of Water Anchored in Multilayered Nanoporous MoS₂ Membranes: Implications for Desalination. *ACS Applied Nano Materials* **2021**, *4*, 10467–10476.
- (58) Abal, J. P.; Barbosa, M. C. Water mobility in MoS₂ nanopores: effects of the dipole–dipole interaction on the physics of fluid transport. *Physical Chemistry Chemical Physics* **2021**, *23*, 12075–12081.
- (59) Abal, J. P.; Bordin, J. R.; Barbosa, M. C. Salt parameterization can drastically affect the results from classical atomistic simulations of water desalination by MoS₂ nanopores. *Physical Chemistry Chemical Physics* **2020**, *22*, 11053–11061.
- (60) Huang, C.; Nandakumar, K.; Choi, P. Y.; Kostiuk, L. W. Molecular dynamics simulation of a pressure-driven liquid transport process in a cylindrical nanopore using two self-adjusting plates. *The Journal of Chemical Physics* **2006**, *124*, 234701.
- (61) Ryckaert, J.-P.; Ciccotti, G.; Berendsen, H. J. Numerical integration of the cartesian equations of motion of a system with constraints: molecular dynamics of n-alkanes. *Journal of Computational Physics* **1977**, *23*, 327–341.

- (62) Lennard-Jones, J. E. Cohesion. *Proceedings of the Physical Society (1926-1948)* **1931**, 43, 461.
- (63) Hummer, G.; Rasaiah, J. C.; Noworyta, J. P. Water conduction through the hydrophobic channel of a carbon nanotube. *Nature* **2001**, 414, 188–190.
- (64) Plimpton, S. Fast parallel algorithms for short-range molecular dynamics. *Journal of Computational Physics* **1995**, 117, 1–19.
- (65) Ostler, D.; Kannam, S. K.; Daivis, P. J.; Frascoli, F.; Todd, B. Electropumping of water in functionalized carbon nanotubes using rotating electric fields. *The Journal of Physical Chemistry C* **2017**, 121, 28158–28165.
- (66) Nosé, S. A molecular dynamics method for simulations in the canonical ensemble. *Molecular Physics* **1984**, 52, 255–268.
- (67) Ge, M.; Sattler, K. Observation of fullerene cones. *Chemical Physics Letters* **1994**, 220, 192–196.
- (68) Smalley, R. E.; Yakobson, B. I. The future of the fullerenes. *Solid State Communications* **1998**, 107, 597–606.
- (69) Fang, C.; Yu, Z.; Qiao, R. Impact of surface ionization on water transport and salt leakage through graphene oxide membranes. *The Journal of Physical Chemistry C* **2017**, 121, 13412–13420.
- (70) Konatham, D.; Yu, J.; Ho, T. A.; Striolo, A. Simulation insights for graphene-based water desalination membranes. *Langmuir* **2013**, 29, 11884–11897.